Modern Physics Letters B
1750264 (11 pages)

DOI: 10.1142/S0217984917502645

Structural study of monoclinic TiO_2 nanostructures and photocatalytic applications for degradation of crystal violet dye

Muhammad T. Amin* and Abdulrahman A. Alazba†

Alamoudi Water Research Chair, King Saud University, Riyadh 11451, Kingdom of Saudi Arabia
*mtamin@ksu.edu.sa
†alazba@ksu.edu.sa

Received 14 March 2017
Revised 30 June 2017
Accepted 3 July 2017
Published 1 August 2017

In this study, titanium dioxide was synthesized by using a hydrothermal technique at different growth temperatures. The study involved investigating the effects of growth temperature on crystal structure, surface area, morphology, and photocatalytic properties. The results indicated the growth of pure monoclinic titania. Additionally, an increase in growth temperature led to the formation of nanostructures to form nanowires and nanorods from nanospheres. The findings revealed variations in crystal quality at different growth temperatures. All samples displayed monoclinic crystal structure with the same molarity at different temperatures including 140°C, 160°C, and 180°C. Various parameters were optimized to grow nanowires and nanorods with a monoclinic crystal structure. The planes of the grown nanostructures were same across all the samples. The grown nanostructures were applied in the degradation of a crystal violet (CV) dye that is also used in optical applications. The study involved demonstrating the excellent photodegradation properties of CV by using a synthesized nanophotocatalyst and providing a detailed discussion on the effects of morphology and crystal structure with respect to photocatalytic properties. The findings also revealed the improved photocatalytic results with respect to nanostructures due to the presence of a broad light harvesting region and the lifetime of the photogenerated electron–hole pair.

Keywords: Crystal violet; monoclinic; photodegradation; temperature; titanium dioxide.

1. Introduction

There is a significant increase in the need for improved living standards due to population and economic growth. This in turn is responsible for several environmental effects including air and water pollution. Additionally, industrial waste is mainly produced by industries that primarily focus on the production of goods and typically ignores waste by-products. This leads to pollutants that can be organic

or inorganic in water. This is a severe problem and researchers adopted different approaches to solve the issue. However, most extant studies used techniques that utilize sunlight to degrade pollutants.

It is extremely important to efficiently use solar energy since this significantly impacts future science and technological applications.[1–5] An example of the potential use of these applications includes photodegradation of organic and inorganic water pollutants, and this has attracted extensive research interest with respect to the use of titania nanostructures.[6–9] The increase in research occurred following the success of a photocatalysis experiment of TiO_2 in a study by Fujishima in 1972.[10] Extensive studies focused on improving the efficiency of photocatalysis.[11–14]

Photocatalysis is a process that accelerates catalysis under the irradiation of light. It was first reported in 1839.[15] The phenomena of photocatalysis can be explained in an extremely simple manner, and it is defined as a phenomenon in which a photon radiates energy that equals or exceeds the energy of the material used as a photocatalyst. This causes the electron to jump from the valence band to conduction band leading to the generation of an electron–hole pair. The photogenerated electrons and holes move to the surface of the photocatalyst; reduction occurs due to electrons and oxidation occurs due to the presence of holes, and this degrades the dye as shown in Fig. 1. Hence, the fore-mentioned process is based on the lifetime of the photogenerated electron–hole pair and the available reactive area of the photocatalyst that can be tuned by selecting an appropriate nanostructure.

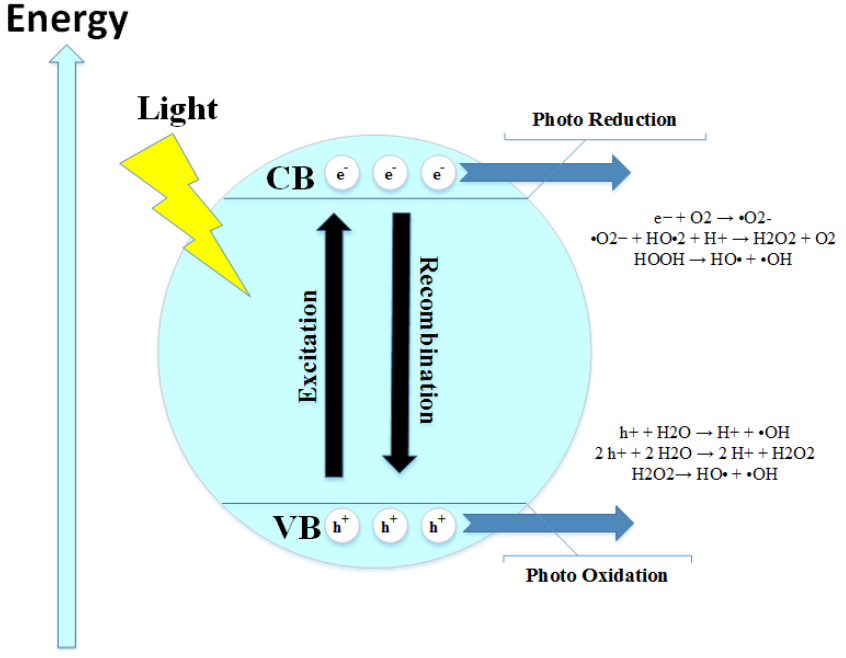

Fig. 1. Schematics of the principle of photocatalysis.[16]

Specifically, TiO_2 is widely used for optical application due to its wide band gap of 3.2 eV. The activation of TiO_2 requires a photon with energy equal to or exceeding its band gap such that the required wavelength of the photon lies in the ultraviolet range of solar light that only corresponds to 8% of the total solar spectrum when compared to 45% of visible region. Thus, researchers performed several studies by introducing doping of transition metals in TiO_2 (Refs. 17–19) to increase the photon to electron–hole generation ratio using TiO_2 nanostructures. However, this includes several drawbacks such as thermal instability and the phenomenon wherein metal centers act in a manner similar to electron trappers leading to low efficiency photocatalysis. An alternate approach for enhancing photocatalytic efficiency of TiO_2 nanostructures involves growing TiO_2 composites with certain other oxides or sulfides such as ZnO, ZnS, and CdS. The disadvantage of the dopant and composites corresponds to the reduction in the lifetime of a photogenerated electron–hole pair. Therefore, a prime focus includes increasing the efficiency of the TiO_2 photocatalyst by decreasing its band gap. A few studies reported a reduction in the band gap when anionic species were introduced as opposed to metal dopants and indicated the effectiveness of introducing the fore-mentioned species. The *p*-state of nitrogen narrowed the band gap as it mixed with the $2p$ states of O.[20] Thus, in order to increase the efficiency of the TiO_2 photocatalyst, it is necessary to decrease either the band gap or increase the lifetime of a photogenerated electron–hole pair.

Several researchers usually use anatase or rutile TiO_2 nanostructures as photocatalysts. Kim *et al.* used anatase TiO_2 nanostructures with different morphologies ranging from rod like one-dimensional (1D) nanostructures to hedgehog-like three-dimensional (3D) hierarchical nanostructures for the degradation of pollutants.[21] Sanz *et al.* synthesized rutile TiO_2 nanostructures and used the same to degrade methylene blue (MB).[22] Nevertheless, this study focuses on TiO_2 nanostructures with a different crystal structure that is termed as a "monoclinic" structure. To our knowledge, monoclinic TiO_2 was rarely studied for degradation of organic dyes.[23] Although, monoclinic TiO_2 shows higher visible light absorption, its efficiency under visible light needs to be further investigated to achieve higher absorption and rapid charge transfer which may result in longer lifetime of charge carriers to achieve enhanced photocatalytic activity.

2. Experimental Procedure

A simple method involving a hydrothermal technique was used in the study to synthesize the nanostructures. It was first reported in a study by von Schafhäutl in 1845[24] in which quartz crystals were synthesized in a pressure cooker. The technique involved performing the growth in hot water at a high temperature. The apparatus consisted of a steel pressure vessel termed as an autoclave. Its advantages include growing nanostructures with nutrients possessing high vapor pressure and growing the crystalline phase despite the disadvantage of unavailability of online monitoring

during the reaction. This study synthesized monoclinic TiO_2 by modifying the growth conditions reported in a study by Sun *et al.*[25]

Autoclaves with a volume corresponding to 100 mL were used. Three samples, with each sample containing 70 mL of deionized water, were used with a molarity of 12 M. Additionally, NaOH was used to maintain the molarity of the solution. Subsequently, 800 mg of TiO_2 (P25 anatase) was mixed in each solution and all the solutions were stirred for 30 min. This was followed by keeping samples A, B, and C in an oven at temperatures corresponding to 140°C, 160°C, and 180°C, respectively. The three samples were kept in an oven for 72 h. The furnace was allowed to cool naturally following the dwell time. This was followed by washing the samples with 0.03 M HCl solution. Finally, the PH of the solution was maintained in a range from 5.5 to 6.5. The samples were then washed with deionized water several times. Finally, the samples were washed with ethanol and were kept in an oven at 56°C overnight. All three samples were annealed at 400°C for 90 min in air in order to improve the crystallinity of the growth structures.

A metal halide lamp with a power of 400 W was used to check the photocatalytic properties of the photocatalyst. Additionally, 10 mg of Titania was poured in a solution that consisted of 50 mL of crystal violet (CV) dye with 0.025 mM solution. The solution was subjected to ultrasonic treatment at 40 kHz for 10 min and was subsequently stirred for 20 min. This was followed by switching on the lamp and performing the photocatalysis experiment for 60 min.

In order to observe the morphology of the grown nanostructures, a Tescan Vega 3 Scanning electron microscope (SEM) was used. The working distance was maintained in the range of 11 mm to 14 mm. The crystal structure of the powdered nanostructures was determined via powder X-ray diffraction (XRD) by using a Rigaku (miniflex) diffractometer with CuKα radiation (1.5406 Å) operated at 40 KV and 40 mA. The scanning step corresponded to 0.02° within the range of 20° to 80° in the 2-theta scan. In order to observe the bonds of the structure, Fourier transform infrared microscopy (FTIR) was performed by using the "Bruker alpha FTIR with ZnSe ATR crystal". The absorption spectrum of TiO_2 was analyzed at room temperature in air using a T-80 ultraviolet–visible (UV–Vis) spectrophotometer of PG instruments. The spectral resolution was maintained at 1 nm in the spectral region of interest. Deionized water was used as a base material to prepare the liquid solution of the nanostructures.

3. Results and Discussions

3.1. *Characteristics of synthesized nanostructure*

3.1.1. *Scanning electron microscopy*

As shown in Fig. 2(a), only a few nanowires exist in conjunction with the nanospheres, and the growth of TiO_2 nanowires did not occur at most of the available sites in sample A. Sample B includes high density nanowires that resembled

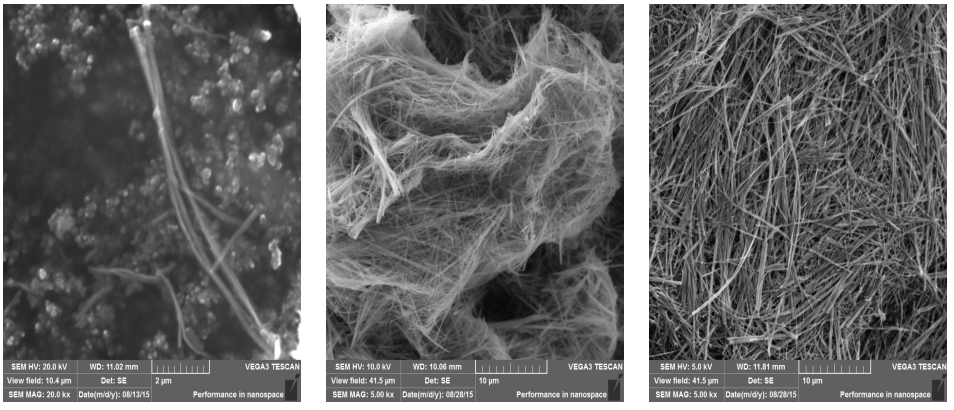

(a) (b) (c)

Fig. 2. SEM images of three samples: (a) nanospheres, (b) nanowires and (c) nanorods.

a mesh of nanowires as shown in Fig. 2(b). As shown in Fig. 2(c), only high density nanorods are observed in the case of sample C. As shown in Fig. 2(b), there is a mixed morphology with nanowires and nanorods. Wires and rods were observed with high lengths ranging up to 13 μm. Thus, an increase in the growth temperature overcomes all parameters that are required for the growth of nanostructures to occur. The temperature increased from 120°C to 140°C, and this led to a high density of nanowires with an average diameter of 120 nm while the length of the nanowires ranged up to several micrometers. With respect to sample C, it was observed that the nanostructures corresponded to nanorods and that a few of the nanorods were fused with one another leading to the formation of nanobelt-type structures. With respect to an end, the structures resembled V shape structures that were fused with each other. However, from the opposite end, the structures resembled two independent nanorods. Thus, the high temperature was not suitable for the required nanostructures because high temperatures resulted in a low surface area of the nanostructures.

3.1.2. *X-ray diffraction*

In this study, XRD was performed to analyze the crystal structure and lattice deformation of the grown nanostructures. The most favorable growth plane was (301) for all samples. The second favorable growth plane for samples A and B corresponded to (−420) while (−123) plane corresponded to the second favorable plane for sample C as shown in Fig. 3. A peak related to sodium presence in the material was observed, and its growth plane corresponded to (−317). All the peaks related to titania displayed a monoclinic crystal structure. The peaks were matched with the reference JCPDS card number "01-075-0552" with ±0.01 Å difference of "*d*" spacing from the *d* spacing mentioned in the reference card. An increase in the growth temperature decreased the crystallinity of the crystal structure especially

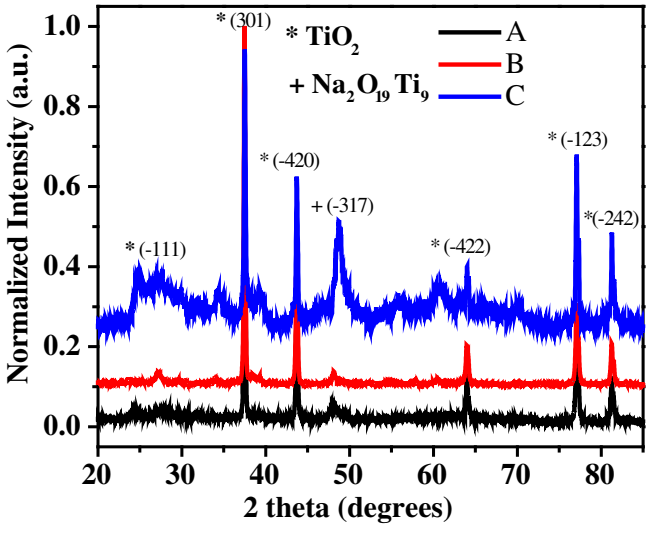

Fig. 3. (Color online) XRD patterns of all samples at various growth temperatures.

with respect to temperatures above 150°C. The full width half maximum (FWHM) of dominant peaks clearly indicated that the crystal quality of samples A and B was significantly higher than that of sample C. This could be attributed to the growth speed that is significantly higher for the sample C when compared with the rest of the two samples. The main reason could be attributed to the high growth temperature that causes high pressure inside the autoclave. The high temperature and high pressure play key roles in growth kinetics. A peak was observed, and it represented the $Na_2Ti_9O_9$ presence. The peak depicts that sample C contains a higher relative percentage of $Na_2Ti_9O_9$ when compared with the samples grown at a lower temperature.

3.1.3. *Fourier transform infrared microscopy*

In this study, FTIR was performed at room temperature and is shown in Fig. 4. A broad band was observed between 3800 cm^{-1} and 3000 cm^{-1}, and this was attributed due to the stretching of O–H bond. After sample growth using hydrothermal reactors, all solutions were washed with deionized water and this process was repeated several times in order for O–H bonds to be observed in FTIR results, as reported in previous studies as well.[26] It indicates the presence of moisture in the samples.[9] A sharp peak at a vibration frequency of 1640 cm^{-1} is also a characteristic of the hydroxyl group.[27] Vibration peaks at a low frequency between 950 cm^{-1} and 600 cm^{-1} were assigned to the stretching of the Ti–O bond.[28] Typically, strong vibration frequency peaks were observed between 700 cm^{-1} and 600 cm^{-1} for samples B and C. An increase in the growth temperature of the nanostructures increase the integrated intensity of the peaks representing the vibration of O–H bonds.

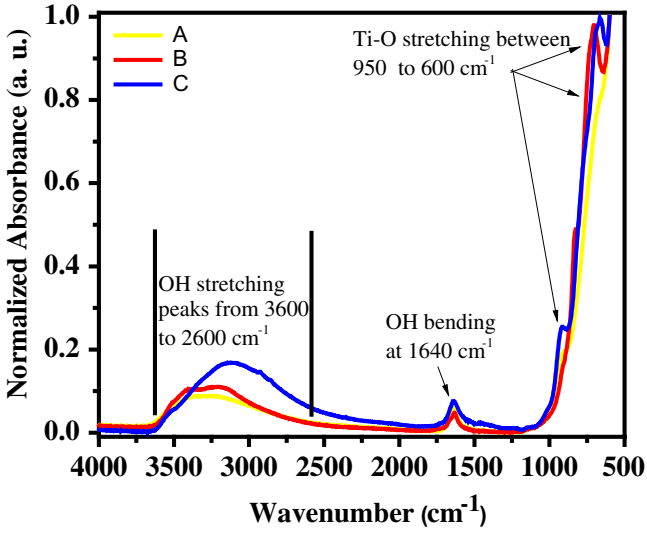

Fig. 4. (Color online) FTIR of the samples with different growth temperatures.

3.1.4. *Ultraviolet–visible spectroscopy*

The UV–Vis absorption spectroscopy results confirmed the TiO_2 absorption. Peaks were obtained at 300 nm, 366 nm, and 391 nm (Fig. 5). All the peaks correspond to the TiO_2 as reported in a study by Dalai *et al.*[29] The findings revealed an excellent absorbance of sample A in the visible range. Sample A displayed good absorbance results in UV range. However, the absorbance of Sample A was slightly lower when

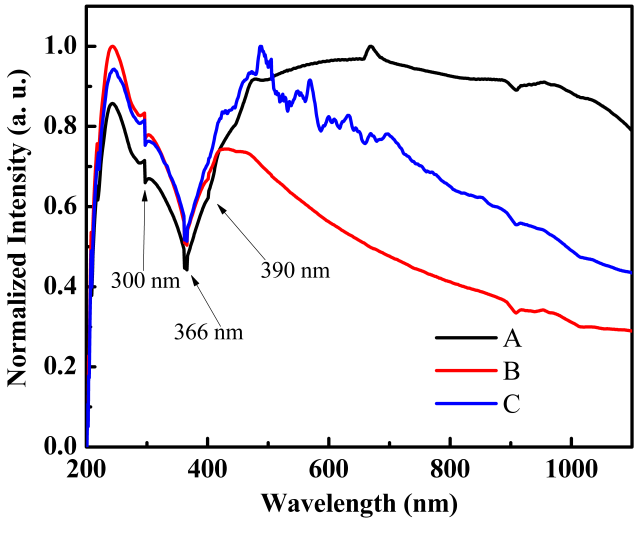

Fig. 5. (Color online) UV–Vis absorption spectroscopy of samples A, B, and C.

compared with the other two samples. The findings indicated significant absorbance throughout the spectrum, and the absorbance reduced after 1000 nm. These types of significantly efficient absorbance results may lead to novel photocatalytic activity due to a large harvesting spectrum of solar light. In contrast, with respect to sample B and sample C, the absorbance in the UV region was excellent and even exceeded that of sample A although the absorbance in the visible range of sample B was lower than that of sample C.

3.1.5. *Photodegradation of CV*

It should be noted that CV is a dye that is used in textile industry with an absorption peak corresponding to 590 nm.[30] The photodegradation of CV is demonstrated by using all samples including Degussa $p25$ as the reference as shown in Figs. 6(a)–6(d).

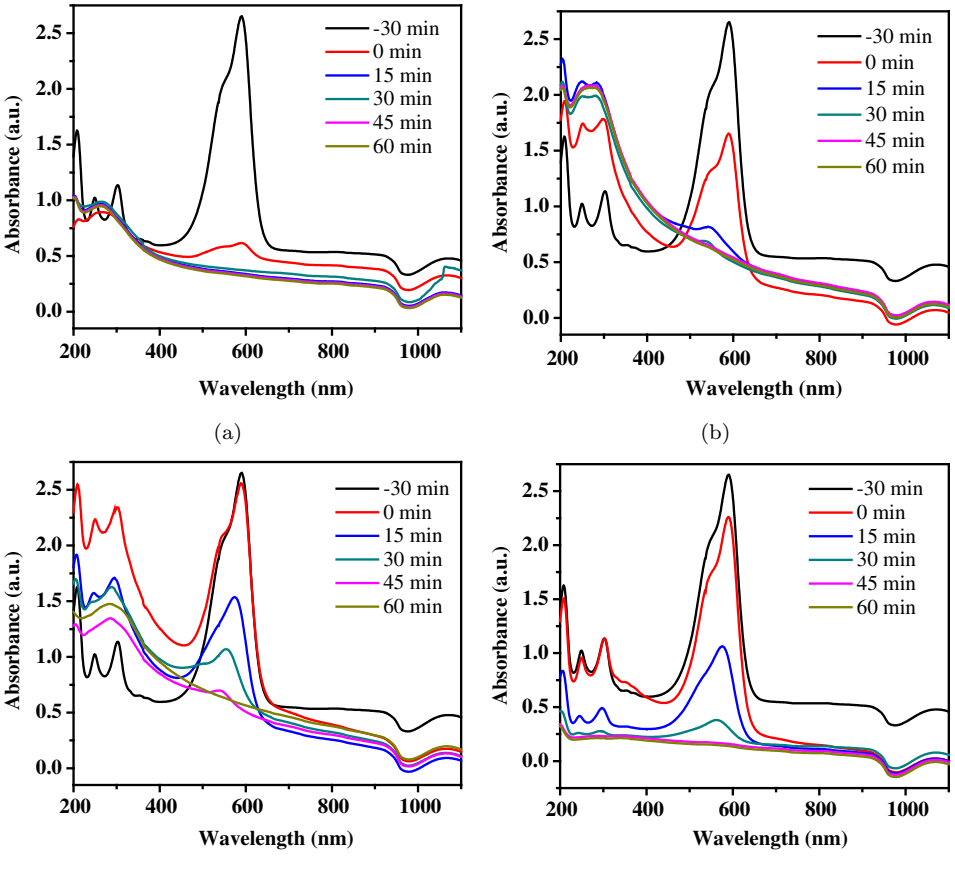

Fig. 6. (Color online) UV–Vis absorption spectroscopy of CV using titania nanostructures for (a) sample A, (b) sample B and (c) sample C, and (d) using Degussa $p25$ as photocatalyst.

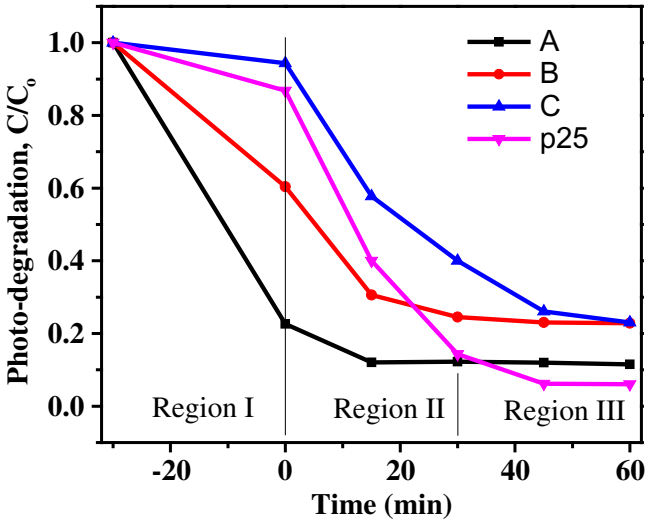

Fig. 7. (Color online) Photodegradation of CV using samples A, B, C, and Degussa *p*25.

The first observation was obtained 30 min prior to starting the experiment, and subsequently, the second observation was obtained after stirring and ultrasonic treatment and this region is presented as region I in Fig. 7 while region II and III ranged from 0 min to 30 min and from 30 min to 60 min, respectively. Four measurements were subsequently obtained at intervals corresponding to 15 min. The results indicated that sample A exhibited excellent photodegradation results in region I followed by the photodegradation results of sample B, sample C and Degussa *p*25, as shown in Fig. 7.

A potential reason corresponded to the monoclinic structure of sample B that also possesses good crystallinity. In region II, sample B was saturated and performed at its maximum possible efficiency. Sample C displayed the average results when compared to those of sample B and Degussa *p*25. This could be due to low crystallinity and the availability of lower surface area due to large-dimensional nanostructures. In region III, Degussa *p*25 showed more efficient photodegradation followed by samples A, B and C. The underlying reason for low performance of sample C can be the attachment of Na to the titania due to high growth temperature. Significant results were observed with respect to sample A in which CV was degraded even during stirring and at very low room light intensity. With respect to the photodegradation results, maximum degradation was reached within 15 min after the experiment commenced which leads sample A as better photocatalyst for the degradation of CV than Degussa p25. The parameters responsible for the highly efficient photodegradation results with respect to sample A include high crystallinity (as shown in XRD results), high surface to volume ratio (as shown in the SEM images), and absorption of both UV visible and infrared light from 200 nm to 1000 nm (as shown in UV–Vis absorption spectroscopy). Thus, it is

concluded that samples synthesized in the study exhibited fast photocatalytic results under sunlight with respect to the degradation of CV. Optimal results can be selected as per requirements that can include photodegradation results of either sample A or sample B. Sample B displayed low absorbance in a visible range when compared with sample C. However, it displayed good photocatalytic results due to high crystallinity. Furthermore, previous studies reported that the low absorbance in a visible range increases the lifetime of photogenerated electron–hole pairs of crystalline nanowires.[31] Nevertheless, this study, in addition to obtaining superior results, also provides a better understanding of the underlying phenomena.

4. Conclusions

In this study, TiO_2 nanospheres, nanowires, and nanorods were successfully synthesized by using a hydrothermal technique for growth. The results indicated that variations in the growth temperature resulted in a significant difference in the morphology. The XRD results revealed that the grown nanostructures displayed monoclinic crystal structures that were optimized with the help of growth conditions. The FTIR results indicated hydroxyl group bond vibrations and titania bond stretching. High crystallinity played a significant role in increasing the lifetime of photogenerated electron–hole pair that led to photocatalysis at high speed. The findings suggested the potential of selecting growth conditions to grow the required nanostructures that include high crystallinity and increased lifetime of photogenerated electron–hole pairs. The results indicated low photocatalytic efficiency and low lifetime of the photogenerated electron–hole pair, and this could be attributed to low crystallinity. In the study, sample A (corresponding to 140°C) displayed the best performance when compared with the rest of the samples, and this is potentially due to the high surface to volume ratio and high crystallinity.

Acknowledgments

This project was funded by the National Plan for Science, Technology and Innovation (MAARIFAH), King Abdulaziz City for Science and Technology, Kingdom of Saudi Arabia, Award Number (11-WAT1875-02).

References

1. C. Li, T. Ahmed, M. Ma, T. Edvinsson and J. Zhu, *Appl. Catal. B: Environ.* **138** (2013) 175.
2. X. Guo, C. Chen, W. Song, X. Wang, W. Di and W. Qin, *J. Mol. Catal. Chem.* **387** (2014) 1.
3. L. Wu, J. C. Yu and X. Fu, *J. Mol. Catal. Chem.* **244** (2006) 25.
4. T. P. Chou, Q. Zhang, G. E. Fryxell and G. Z. Cao, *Adv. Mater.* **19** (2007) 2588.
5. H. M. Coleman, B. R. Eggins, J. A. Byrne, F. L. Palmer and E. King, *Appl. Catal. B: Environ.* **24** (2000) L1.
6. X. Wang, Y. Liu, Z. Hu, Y. Chen, W. Liu and G. Zhao, *J. Hazard. Mater.* **169** (2009) 1061.

7. J. Ouyang, M. Chang and X. Li, *J. Mater. Sci.* **47** (2012) 4187.
8. I. V. Kostedt, A. A. Ismail and D. W. Mazyck, *Ind. Eng. Chem. Res.* **47** (2008) 1483.
9. M. M. Ba-Abbad, A. A. H. Kadhum, A. B. Mohamad, M. S. Takriff and K. Sopian, *Int. J. Electrochem. Sci.* **7** (2012) 4871.
10. A. Fujishima and K. Honda, *Nature* **238** (1972) 37.
11. I. S. Cho, Z. Chen, A. J. Forman, D. R. Kim, P. M. Rao, T. F. Jaramillo and X. Zheng, *Nano Lett.* **11** (2011) 4978.
12. Y. Wang, L. Zhang, K. Deng, X. Chen and Z. Zou, *J. Phys. Chem. C* **111** (2007) 2709.
13. E. Formo, E. Lee, D. Campbell and Y. Xia, *Nano Lett.* **8** (2008) 668.
14. I. García-Fernández, I. Fernández-Calderero, M. I. Polo-López and P. Fernández-Ibáñez, *Catal. Today* **240** (2015) 30.
15. E. Bequerel, *C. R. Acad. Sci* **9** (1839) 145.
16. M. A. Johar, R. A. Afzal, A. A. Alazba and U. Manzoor, *Adv. Mater. Sci. Eng.* **2015** (2015) 1.
17. D. H. Kim, D.-K. Choi, S.-J. Kim and K. S. Lee, *Catal. Commun.* **9** (2008) 654.
18. M. M. Rashad, E. M. Elsayed, M. S. Al-Kotb and A. E. Shalan, *J. Alloys Compd.* **581** (2013) 71.
19. M. Khairy and W. Zakaria, *Egypt. J. Pet.* **23** (2014) 419.
20. C. Burda, Y. Lou, X. Chen, A. C. S. Samia, J. Stout and J. L. Gole, *Nano Lett.* **3** (2003) 1049.
21. H.-B. Kim, H. Kim, W. I. Lee and D.-J. Jang, *J. Mater. Chem. A* **3** (2015) 9714.
22. R. Sanz, L. Romano, M. Zimbone, M. A. Buccheri, V. Scuderi, G. Impellizzeri, M. Scuderi, G. Nicotra, J. Jensen and V. Privitera, *J. Appl. Phys.* **117** (2015) 074903.
23. K. K. Paul, R. Ghosh and P. K. Giri, *Nanotechnology* **27** (2016) 315703.
24. K. Byrappa and M. Yoshimura, *Handbook of Hydrothermal Technology* (Cambridge University Press, Cambridge, 2008).
25. K. C. Sun, M. B. Qadir and S. H. Jeong, *RSC Adv.* **4** (2014) 23223.
26. R. Ahmad, M. Mohsin, T. Ahmad and M. Sardar, *J. Hazard. Mater.* **283** (2015) 171.
27. M. Wan, W. Li, Y. Long and Y. Tu, *Anal. Methods* **4** (2012) 2860.
28. V. Žunič, S. D. Škapin and D. Suvorov, *J. Am. Ceram. Soc.* **98** (2015) 2997.
29. S. Dalai, S. Pakrashi, R. S. S. Kumar, N. Chandrasekaran and A. Mukherjee, *Toxicol. Res.* **1** (2012) 116.
30. E. Q. Adams and L. Rosenstein, *J. Am. Chem. Soc.* **36** (1914) 1452.
31. P. Rosenits, T. Roth, S. Reber, W. Warta and S. W. Glunz, Lifetime studies on crystalline silicon thin-films by photoluminescence measurements, in *Proc. 23rd European Photovoltaic Solar Energy Conference* (2008), pp. 2224–2227.